Title

Direct lineage conversion of postnatal mouse cortical astrocytes to oligodendrocyte lineage cells.

Authors

Justine Bajohr[1-2], Erica Y. Scott[1,3-5], Arman Olfat[1], Mehrshad Sadria[5-6], Kevin Lee[1], Maria Fahim[1], Hiba T. Taha[1,2], Daniela Lozano Casasbuenas[1,7], Ann Derham[1], Scott A. Yuzwa[7], Gary D. Bader[5,8], Maryam Faiz[1,2,7 # $]

Affiliations

1. Department of Surgery, Temerty Faculty of Medicine; University of Toronto; Toronto, Ontario, M5S 1A8, Canada
2. Institute of Medical Science, Temerty Faculty of Medicine; University of Toronto; Toronto, Ontario, M5S 1A8, Canada
3. Institute of Biomedical Engineering, Faculty of Applied Science and Engineering; University of Toronto; Toronto, Ontario, M5S 3G9, Canada
4. Department of Chemistry, Faculty of Arts and Science; University of Toronto; Toronto, Ontario, M5S 3G3, Canada
5. Donnelly Centre for Cellular and Biomolecular Research, Temerty Faculty of Medicine; University of Toronto; Toronto, Ontario, M5S 3E, Canada
6. Department of Applied Mathematics, University of Waterloo, Waterloo, Ontario N2L 3G1, Canada.
7. Department of Laboratory Medicine and Pathobiology, Temerty Faculty of Medicine; University of Toronto; Toronto, Ontario, M5S 1A8, Canada
8. Department of Molecular Genetics, Temerty Faculty of Medicine; University of Toronto; Toronto, Ontario, M5S 1A8

#Correspondence: maryam.faiz@utoronto.ca

$Lead contact: maryam.faiz@utoronto.ca

SUMMARY

Oligodendrocyte lineage cells (OLCs) are lost in many CNS diseases. Here, we investigate the generation of new OLCs via ectopic expression of *Sox10*, *Olig2* or *Nkx6.2* in mouse postnatal astrocytes. Using stringent analyses including, Aldh1l1-astrocyte fate mapping and live cell imaging we confirm that *Sox10* and *Olig2*, but not *Nkx6.2*, convert Aldh1l1^{pos} astrocytes to induced OLCs (iOLCs). With single cell RNA sequencing (scRNA-seq) we uncover the molecular signatures of iOLCs. Transcriptomic analysis of *Sox10*- and control cultures over time reveals a clear trajectory from astrocytes to iOLCs. Finally, perturbation models CellOracle and Fatecode support the idea that *Sox10* drives cells towards a terminal iOLC fate. Altogether, this multidimensional analysis shows bonafide conversion of astrocytes to iOLCs using *Sox10* or *Olig2* and provides a foundation for astrocyte DLR strategies to promote OLC repair.

KEYWORDS

Astrocyte, oligodendrocyte, reprogramming, deep learning, single cell RNA sequencing, fate mapping

INTRODUCTION

Oligodendrocytes (OLs) are best known as the myelinating cells of the central nervous system (CNS). OLs ensheath neuronal axons to enable fast propagation of action potentials. Consequently, the loss or dysfunction of OLs results in impaired neurological function that is characteristic of many types of CNS disease and injury. Multiple sclerosis (MS), Alzheimer's Disease, spinal cord injury, white matter stroke and cerebral palsy are all characterized by oligodendrocyte failure. Thus, therapeutic strategies aimed at replacing OLs are of significant clinical interest (1).

Direct lineage reprogramming (DLR) aims to generate new target cells lost to disease via the forced conversion of donor cells. Typically, DLR is performed by the overexpression of transcription factors (TFs). Early pioneering work from the Tesar Lab demonstrated fibroblast to induced oligodendrocyte progenitor cell (iOPC) conversion by ectopic expression of *Olig2*, *Sox10*, and *Nkx6.2*; determinants of OL cell fate in the embryonic brain (2). The combination of *Sox10* and *Olig2* was also later used to generate iOPCs from pericytes (3). Therapeutically, however, these newly generated iOPCs still require transplantation into the brain. Therefore, methods to reprogram endogenous CNS cells would be advantageous.

In parallel, astrocytes, CNS-resident cells, have emerged as donor cells in DLR strategies aimed at generating new neurons (4–7). Astrocytes are an attractive donor cell type for OL conversion given their shared neural origin (8,9). Astrocytes may already have relevant epigenetic marks and active TFs that could make DLR faster or more efficient (10–13). In addition, closely related cells may require fewer TFs for conversion. Indeed, conversion of astrocytes to an induced oligodendrocyte-like cell was suggested using *Sox10* alone (14). Therefore, we reasoned that single 'Tesar' factors, *Olig2*, *Sox10*, or *Nkx6.2,* could be used to force astrocyte conversion to new, induced oligodendrocyte lineage cells (iOLCs).

The OL lineage is comprised of oligodendrocyte progenitor cells (OPCs) that give rise to committed oligodendrocyte progenitors (COPs). These COPs differentiate into mature OLs (mOLs), comprising at least 6 different states (15). Of interest, during OL development, *Olig2, Sox10, and Nkx6.2* show different temporal expression and play different roles in OL fate specification. *Olig2,* long considered an OL lineage fate determinant (16), is also expressed in astrocytes (17,18), which suggests a broad role in early glial commitment (19,20). *Sox10* is important throughout OL development; *Sox10* promotes early OL lineage specification by re-inducing *Olig2* (21) and by inhibiting *Sufu (22)*, but is also required for OL survival following myelination (23,24). In contrast, *Nkx6.2* is expressed late in OL development, with myelin genes *Mbp* and *Mog,* and plays a role in regulating myelination (25,26). Given the unique roles of each of these TFs in development, we further hypothesized that each of these single factors would have varying efficiency in generating iOLCs.

Recent controversy in the field of astrocyte to neuron DLR *in vivo (27)* has highlighted the need for rigorous reporting of DLR outcomes. In a landmark study using astrocyte fate mapping strategies, the authors suggested that off-target transduction of endogenous cells was misrepresented as DLR (27). Therefore, it is important that new DLR paradigms utilize fate mapping, and stringent, multi-faceted analysis to determine the origin of the newly generated cells.

Here, we used lentiviral delivery of *Olig2*, *Sox10*, or *Nkx6.2* to investigate single TF conversion of postnatal (P0-P5) GFAP+ cortical astrocytes to iOLCs. Lineage tracing experiments using Aldh1l1-CreERT2;Ai14 mice confirmed that *Sox10* and *Olig2* directly convert Aldh1l1+ astrocytes to iOLCs. Moreover, live cell imaging, single cell RNA sequencing (scRNA seq) and deep learning methods support the findings that iOLCs can be generated from astrocytes following TF delivery. Altogether, these findings show bonafide astrocyte to iOLC DLR and lay the groundwork for future studies utilizing DLR for diseases involving OLC dysfunction and loss.

METHODS

Animals

All experiments were performed in accordance with approved Animal Use Protocols (AUP 20012151, 25-0389H) from the Division of Comparative Medicine at the University of Toronto. P0-P5 Ai14 **(**B6;129S6- *Gt(ROSA)26Sor*$^{tm14(CAG\text{-}tdTomato)Hze}$/J, RRID:IMSR_JAX:007908) and Ai14;Ald1l1-CreERT2 mice (Ai14 crossed to B6N.FVB-Tg(Aldh1l1-cre/ERT2)1Khakh/J [RRID:IMSR_JAX:031008]) were used to generate postnatal astrocyte cultures.

Cell Culture

Cortical astrocytes were isolated from male and female P0-P5 mice as previously described (28). Briefly, mice were decapitated, followed by the removal of the skull and meninges. Cortices were dissected, pooled, and mechanically dissociated in astrocyte media [DMEM (Gibco Catalogue No. 10569-010), 10% fetal bovine serum (FBS) (Gibco Catalogue No. 10082147) and 1% penicillin/streptomycin (Gibco Catalogue No. 15140122)]. Cells were cultured in flasks pre-coated with 10 µg/ml poly-d-lysine (Sigma Catalogue No. P6407), and incubated at 37˚C, 5% CO2. Media was changed the day following isolation and every other day thereafter. Once the cells reached 80% confluency, typically after 6 days, flasks were placed on an orbital shaker for 30 minutes to remove contaminating microglia. Astrocyte media was replaced. For Ai14;Aldh1l1-CreERT2 cultures, 1uM 4-OHT was added to the astrocyte media at this step. Flasks were returned to the orbital shaker overnight, followed by vigorous shaking for one minute to remove contaminating OLCs. Media was removed and astrocytes were incubated in TrypLE Express Enzyme (Gibco Catalogue No. 12604013) for 5 minutes at 37˚C, 5% CO2 to lift off the astrocytes. To inactivate the enzyme, astrocyte media was added at a 3:1 ratio (media:TrypLE). Cell suspension was collected and centrifuged at 300 x g for 5 minutes. Following removal of the supernatant, the pellet was resuspended in astrocyte media. Cells were then plated on poly-l-ornithine/laminin coated coverslips at either 50,000 or 70,000 cells/well in 24 well plates and incubated at 37˚C, 5% CO2. For live

cell analysis, cells were plated at 10,000 cells/ well in 96 well plates with poly-l-ornithine/laminin coating. For poly-l-ornithine/laminin coating, 0.1mg/ml poly-l-ornithine (Sigma Catalogue No. P4957) was added to dishes overnight at 37˚C, washed 3 times with 1X phosphate buffered saline (PBS), and then dishes were incubated for two hours at 37˚C with 10 µg/ml laminin (Sigma Catalogue No. L2020).

Reprogramming

Lentiviral particles were purchased from VectorBuilder. For Ai14 reprogramming, LV-hGFAP::*Sox10*-P2A-Cre, LV-hGFAP::*Olig2*-P2A-Cre, LV-hGFAP::*Nkx6.2*-P2A-Cre, and control LV-hGFAP::BFP-T2A-Cre were used. For Ai14;Aldh1l1-CreERT2 reprogramming, LV-hGFAP::*Sox10*-P2A-zsGreen, LV-hGFAP::*Olig2*-P2A-zsGreen, LV-hGFAP::*Nkx6.2*-P2A-zsGreen and control LV-hGFAP::zsGreen were used. A multiplicity of infection (MOI) of 100 was used for all experiments. Virus-containing astrocyte media was placed on the cells and left overnight. Viral media was replaced with fresh astrocyte media one day post transduction (DPT). Three DPT, cells were switched to OPC differentiation media (2) [DMEM/F12/Glutamax (Gibco Catalogue No. 11330032), 1X N2 (Gibco Catalogue No. 17502048), 1X B27 without vitamin A (Gibco Catalogue No. 17504044), 200 ng/ml SHH (R&D Systems Catalogue No. 464-SH), 20 ng/ml FGF (R&D Systems Catalogue No. 3139-FB), 4 ng/ml PDGF (Sigma Catalogue No. SRP3228)]. At 10 DPT, the cells were switched to OL differentiation media (2) [DMEM/F12/Glutamax, 1X N2, 1X B27 without vitamin A, 40 ng/ml T3 (T2877 Catalogue No. Sigma), 200 ng/ml SHH, 100 ng/ml Noggin (R&D Systems Catalogue No. 1967-NG), 10 µM cAMP (Sigma Catalogue No. A9501), 100 ng/ml IGF (R&D Systems Catalogue No. 791-MG), 10 ng/ml NT3 (Sigma Catalogue No. SRP6007)].

Live Cell Analysis

Astrocytes isolated from Ai14;Aldh1l1-CreERT2 mice were plated in 96 well plates, transduced and imaged every hour from 7 to 12DPT using the Apotome live cell system (Zeiss). 25 z-stack tiled images per well were captured with brightfield as well as the 488nm and 568nm fluorescent wavelength. Images were stitched to create a continuous video for each well. At 12DPT, cells were fixed and stained for OLC markers to confirm fate. Each well was then re-imaged at this final timepoint and OLC+ reprogrammed cells were matched to the live cell video and retrospectively analyzed for starting cell morphology and fluorescent expression. To characterize starting cell morphology, an analysis was first performed on 70 Aldh1l1+tdTomato+ astrocytes in tamoxifen-labelled Aldh1l1-CreERT2;Ai14 cultures and 70 PDGFRa+ OPCs from iOLC cultures (Table S1). Astrocyte and OPC paramenters were established for cell size, nucleus size, number of branches and branch thickness (Supplemental Figure 1). These parameters were then used to characterize starting cells as astrocytes or OPCs.

Immunocytochemistry

Cells were fixed in 4% paraformaldehyde (PFA) (Sigma Catalogue No. P6148) for 20 minutes followed by three washes with 1X PBS. Cell membranes were permeabilized with 0.1%

129 Triton-X-100 (Sigma Catalogue No. X100) for 10 minutes at room temperature, followed by
130 three washes with 1X PBS, and then blocked with 5% milk for one hour at room temperature.
131 Cells were incubated with primary antibodies in 1X PBS overnight at 4°C, washed three times
132 with 1X PBS, and then incubated with secondary antibodies and DAPI (Sigma Catalogue No.
133 D9542) in 1X PBS at room temperature for one hour. Following three final 1X PBS washes,
134 coverslips were mounted on glass slides (Fisher Scientific Catalogue No. 125523)
135 with Mowiol mounting solution (Sigma Catalogue No. 81381). For staining of membrane
136 bound proteins (O4, PDGFRα), no permeabilization step with Triton-X-100 was performed.
137 Primary antibodies: mouse anti-SOX10 (RRID:AB_10844002, 1:250), rabbit anti-PDGFRα
138 (RRID:AB_2892065, 1:500), mouse anti-O4 (RRID:AB_357617, 1:1000) and rat anti-
139 MBP RRID:AB_305869, 1:50).
140 Secondary antibodies: anti-mouse IgG 488 (Invitrogen Catalogue No. A32723) and 647
141 (Invitrogen Catalogue No. A32728), anti-mouse IgM heavy chain 488 (Invitrogen Catalogue
142 No. A21042) and 647 (Invitrogen Catalogue No. A21238), anti-rabbit 488 IgG (Invitrogen
143 Catalogue No. A11034) and 647 (Invitrogen Catalogue No. A32733), anti-rat IgG 488
144 (Invitrogen Catalogue No. A21208) and 647 (Invitrogen Catalogue No. A21247) all at 1:1000.
145
146 **Microscopy and Image Analysis**
147 Fluorescent images for quantification were taken on an LSM 880 Elyra Superresolution and
148 LSM 900 (Zeiss) using a 20x objective and Zen Blue software (Zeiss). Post-acquisition linear
149 adjustments of brightness for all channels were made to micrographs using the Zen Blue
150 software in Figure 1C, Figure 2E-G and Supplemental Figure 5D. For quantification, ten
151 regions of interest were selected at random for each well. Images were analyzed using
152 ImageJ software (National Institutes of Health, RRID:SCR_003070). Reprogramming
153 efficiency was calculated as a measure of total OLC marker$^+$reporter$^+$DAPI$^+$ cells over
154 total reporter$^+$DAPI$^+$cells.
155
156 **scRNA-seq capture and processing**
157 At 14DPT, LV-hGFAP::*Sox10*-P2A-Cre, LV-hGFAP::*Olig2*-P2A-Cre, LV-hGFAP::*Nkx6.2*-P2A-
158 Cre, and control LV-hGFAP::BFP-T2A-Cre cultures were processed using the BD Rhapsody
159 System (BD Biosciences) and then sequenced. For single-cell isolation, an average
160 of 9813.75 viable cells were captured in wells at cell load (Table S2). The BD Rhapsody
161 scanner reported an average multiplet rate of 10.13% and an average number of wells with
162 viable cells and a bead of 7081.5 (Table S2). Detailed metrics for each sample can be found
163 in Table S2. Samples were down-sampled to 2500 cells and carried through and converted
164 to cDNA using the BD Rhapsody WTA Reagent Kit (Becton Dickinson Canada, Catalogue No.
165 633802). Each cell was sequenced at approximately 100 million reads per cell (at least
166 2x150 bp paired-end reads) on a Novaseq (Donnelly Sequencing Centre, University of
167 Toronto).
168 In addition, LV-GFAP::*Sox10* and control LV-GFAP::Cre cultures were collected prior to
169 transduction, at 3DPT and 8DPT, and processed using the BD Rhapsody System (BD
170 Biosciences) and then sequenced. For single-cell isolation, an average of 10263.8 viable
171 cells were captured in wells at cell load (Table S3). The BD Rhapsody scanner reported an
172 average multiplet rate of 6.86% and an average number of wells with viable cells and a bead

of 7785 (Table S3). Detailed metrics for each sample can be found in Table S3. Samples were down-sampled to 2500 cells and carried through and converted to cDNA using the BD Rhapsody WTA Reagent Kit (Becton Dickinson Canada, Catalogue No. 633802). Each cell was sequenced at approximately 100 million reads per cell (at least 2x150 bp paired-end reads) on a Novaseq (Donnelly Sequencing Centre, University of Toronto).

scRNA-seq analysis

Fastq files were first demultiplexed with Kallisto (29) (RRID:SCR_016582)(v0.48.0) and Bustools (30) (RRID:SCR_018210)(V 0.41.0) using supplied whitelists (Data S1) with the -BDWTA option and aligning to GRCm38.96 with Cre sequence appended to the end. Bustools (30) was then used to generate gene count tables. Cells were plotted based upon UMI counts per barcode, thresholds were selected based on inflection point of UMI count per barcode plots. These thresholds produced read and gene count distributions that were comparable between all treatment groups (Supplemental Figure 2A, Supplemental Figure 6A). Gene count tables were made into S4 objects, scaled, normalized and dimensions reduced (PCA then UMAP) using the Seurat (31) package (RRID:SCR_016341) (v4.1). Clusters identified as microglia and as vascular and leptomeningeal cells (VLMCs) (Supplemental Figure 2B-C [cluster 8], Supplemental Figure 6B-C [cluster 6 and 8]) were removed prior to further analysis.

Gene markers for oligodendrocyte lineage cells were adopted from studies observing *in vivo* mouse oligodendrocyte lineage cells across several areas in young and mature CNS tissues (15). These markers were converted into percent expression of each UMAP cluster using the PercentageFeatureSet function from Seurat (31), with further gene resolution displayed by heatmaps created using ComplexHeatmap (32)(RRID:SCR_017270) (v12.13.1). An additional set of gene markers, demonstrating similar, but less resolved, conclusions was also used from an *in vitro* rat study looking at OLCs from the cortex (33). Stacked violin cluster dot plots were made with scCustomize (34)(RRID:SCR_024675)(v2.1.2). For pseudotime and trajectory analysis Slingshot (35) (RRID:SCR_017012)(v2.3.1) and Monocle3 (36–40) (RRID:SCR_018685) were used. For *in silico Sox10* perturbation, CellOracle (41) (v0.14.0) was used. Plots were produced using ggplot2 (42) (RRID:SCR_014601)(v3.3.5) and figure generating scripts were run in R studio (43) (v4.2.0), with demultiplexing using Kallisto (29) and Bustools (30) run on a Compute Canada HPC cluster. All scripts used for processing of scRNA-seq data and for figure generation can be found at github.com/eyscott/Bajor_BDRhapsodyData_DLR.

Deep-learning analysis

Fatecode (44) was used to identify key genes for cellular transition. To optimize the autoencoder and subsequent classifier configuration, a grid search was conducted to systematically evaluate various combinations of hyperparameters. These included: latent layer size, number of nodes in the first and second layers of the autoencoder, classifier architecture, and type of activation function. The grid search aimed to identify the hyperparameters that minimized a combined reconstruction and classification loss function, signifying the optimal performance for our specific dataset. Perturbations on the

latent space were performed and cell classifications as well as genes associated with each perturbation were obtained.

Statistical Analysis

Percentage values were transformed using the arcsine square root transformation and assessed for normal distribution using the Shapiro-Wilks test. When distribution and variance were equal, a matched pairs one-way ANOVA ([Ai14:D8, D10, D12 O4, D12 MBP], [Ai14;Aldh1l1-CreERT2: D12 MBP zsGreen+, D12 MBP tdTomato+) or one-way ANOVA ([Ai14:D14], [Ai14;Aldh1l1-CreERT2: D12 MBP zsGreen+,tdTomato+]) , or paired t-test ([Ai14;Aldh1l1-CreERT2: D12 PDGFRα zsGreen+tdTomato+, D12 PDGFRα tdTomato+, O4 zsGreen+, O4 tdTomato+]) was performed to compare reprogramming efficiency of TF groups to a control group (Ai14: LV-GFAP::Cre, Ai14;Aldh1l1-CreERT2: LV-GFAP::zsGreen). When transformed values did not follow a Gaussian distribution, a Kruskal-Wallis test (Ai14: D12 PDGFRα, D14 PDGFRα) or Wilcoxon test (Ai14;Aldh1l1-CreERT2: PDGFRα zsGreen+, O4 zsGreen+tdTomato+) was performed to compare reprogramming efficiency to a control group (Ai14: LV-GFAP::Cre, Ai14;Aldh1l1-CreERT2: LV-GFAP::zsGreen). In both cases, Dunnett's post-hoc testing was performed to correct for multiple comparisons. Differences were considered significant at $p < 0.05$. Values are presented as mean ± SEM. The statistical software used for transformation, distribution, variance, ANOVA, Kruskal-Wallis, t-test, Wilcoxon test and Dunnett's analysis was GraphPad Prism version 9.0.1 (RRID:SCR_002798).

RESULTS

iOLCs are generated following expression of *Olig2*, *Sox10* or *Nkx6.2*

To investigate astrocyte to OLC conversion, we established postnatal, cortical astrocyte cultures from Ai14 mice. To understand the purity of our cultures, we quantified the numbers of contaminating OLCs. Quantification of SOX10+, O4+ and MBP+ OLCs showed less than 2.5% in our cultures (Supplemental Figure 3A).

To examine the reprogramming potential of *Olig2, Sox10,* and *Nkx6.2*, we transduced Ai14 astrocytes with either LV-GFAP::*Olig2,* LV-GFAP::*Sox10*, LV- GFAP::*Nkx6.2* or a control LV-GFAP::*Cre* (Figure 1A). When we quantified the numbers of tdTomato+ cells that co-expressed OPC (PDGFRa), COP (O4) or OL (MBP) markers at 8 and 10 DPT, no differences were seen in any of the TF-transduced cultures compared to controls (Figure 1B). By 12 DPT, *Olig2*- cultures showed an increase in the percentage of tdTomato$^+$PDGFRα$^+$ OPCs ($p = 0.0309$, H-statistic: 7.514), whereas *Sox10*- and *Nkx6.2*- cultures showed an increase in tdTomato$^+$MBP$^+$ OLs (*Sox10:* $p = 0.0004$, *Nkx6.2:* $p = 0.0108$, F statistic = 13.28, degrees of freedom =3) (Figure 1B-C). No differences were seen in the percentage of tdTomato$^+$O4$^+$ COPs in any condition at 12DPT (Figure 1B). However, by 14DPT we observed an increase in the percentage of tdTomato$^+$O4$^+$ COPs in *Sox10*- cultures when compared to controls ($p = 0.0213$, F statistic = 3.512, degrees of freedom = 3) (Figure 1B-C). Finally, to understand whether a longer time in culture could increase the number of MBP+ OLs, we cultured cells for an additional 8 days and analyzed the percent of tdTomato$^+$MBP$^+$ cells at 22 DPT. No differences were seen in tdTomato$^+$MBP$^+$ OLs in any condition compared to

controls (Supplemental Figure 3B). Altogether, these findings suggest that *Olig2*, *Sox10* and *Nkx6.2* increase the percentage of iOLCs relative to controls in Ai14 astrocyte cultures.

Canonical OLC cluster found in TF-treated cells following scRNA-seq

To further characterize *Olig2-, Sox10-, Nkx6.2-* and control cultures, we performed scRNA-seq at 14DPT (Figure 1A). Clustering analysis showed the appearance of nine clusters (Figure 1D). We then used proportion analysis to identify clusters that were unique to TF-treated samples. Clusters 3 and 8 were predominantly comprised of cells from TF-induced cultures (Figure 1E-F). The top 10 genes marking each cluster in Figure 1D are highlighted in Figure 1G. Canonical OLC genes such as *Mbp, Plp1, Bcas1* and *Cldn11* were expressed in clusters 3 and 8 (Figure 1G), further suggesting that the increase in iOLCs is a result of TF delivery.

Next, we compared the molecular profiles of clusters 3 and 8 to established OL lineage datasets. First, we used OLC specific annotations of mouse fetal and adult OLCs derived from Marques *et al* (15) to bin the data. We found that cluster 3 was characterized by COP signatures, while cluster 8 was characterized by COP, newly formed oligodendrocyte (nfOL) and myelin forming oligodendrocyte (mfOL) signatures (Supplemental Figure 4A). We also used OLC annotations of *in vitro* OLCs derived from Dugas *et al* (33) to bin the data. Again, we saw that cluster 8 was characterized by OL signatures, but cluster 3 was not. (Supplemental Figure 4B). Altogether, these findings further support the observation of increased OLC generation in TF-induced Ai14 cultures (Figure 1B).

Bonafide astrocyte to OLC conversion is confirmed with astrocyte fate mapping.

We had previously observed contaminating OLCs in our cultures and the presence of tdTomato$^+$OLC marker$^+$ cells in our Cre controls. Therefore, to confirm the origin of these newly generated OLCs, we performed astrocyte fate mapping using Ai14;Aldh1l1-CreERT2 cultures, the current gold standard in the field (27). Prior to transduction, post-natal cortical Ai14;Aldh1l1-CreERT2 astrocyte cultures were treated with 1uM 4-OHT to permanently label all *Aldh1l1* expressing cells with tdTomato (Figure 2A). Cultures were transduced with LV-GFAP::*Sox10*-zsGreen, LV-GFAP::*Olig2*-zsGreen, LV-GFAP::*Nkx6.2*-zsGreen or a LV-GFAP::zsGreen control (Figure 2A). Any OLCs that were directly converted by a TF from these *Aldh1l1* expressing astrocytes would therefore express zsGreen and tdTomato (Figure 2A). To understand whether the OPCs generated from *Olig2* overexpression were the product of astrocyte reprogramming, we quantified the percentage of PDGFRα+zsGreen$^+$tdTomato$^+$ cells at 12DPT. We observed an increase in PDGFRα$^+$zsGreen$^+$tdTomato$^+$ OPCs compared to controls, confirming the astrocytic origin of iOPCs (Figure 2B,E). To assess the origin of *Sox10*-induced COPs we quantified the percentage of O4$^+$zsGreen$^+$tdTomato$^+$ cells at 14DPT. No increase was observed in *Sox10* cultures compared to controls (Figure 2C). Finally, to determine the origin of OLs generated by *Sox10* or *Nkx6.2,* we quantified the percentage of MBP$^+$zsGreen$^+$tdTomato$^+$ OLs at 12DPT. We observed an increase of MBP$^+$zsGreen$^+$tdTomato$^+$ OLs generated by *Sox10*, but not from *Nkx6.2* (Figure 2D,F). This

305 suggests that *Olig2* and *Sox10* reprogram *Aldh1l1* astrocytes to iOLCs, while *Nkx6.2*-derived
306 OLs and *Sox10*-derived COPs previously observed (Figure 1B), are not the result of *Aldh1l1*
307 astrocyte conversion. To further confirm these findings, we performed live cell imaging
308 of Ai14;Aldh1l1-CreERT2 *Sox10*-treated and control cultures from 7DPT to 12DPT. At 12DPT,
309 we observed tdTomato^{+}zsGreen^{+} cells that co-expressed OLC markers (PDGFRa/O4/MBP+)
310 and showed OPC-like morphologies (small nucleus, multiple thin branches) (Figure 2G,
311 Supplemental Figure 1). When we tracked these cells back to 7DPT, we found that they
312 showed a characteristic astrocyte morphology (large cell body and nucleus, with minimal
313 branching) (Figure 2G, Supplemental Figure 1, Supplemental Video 1). Taken together, these
314 findings further demonstrate bonafide astrocyte to iOLC conversion.
315
316 We also examined the numbers of Aldh1l1^{+} non-transduced (tdTomato^{+}only) cells, as well
317 as Aldh1l1^{neg} virally transduced (zsGreen^{+} only) cells (Supplemental Figure 5). No difference
318 in the percentage of OLC marker^{+}tdTomato^{+}zsGreen^{neg} was seen between TF-treated and
319 control cultures (Supplemental Figure 5). However, when we examined
320 zsGreen^{+}tdTomato^{neg} cells, we observed an interesting increase in the percentage of
321 MBP^{+}zsGreen^{+}tdTomato^{neg} OLs at 12DPT in *Sox10*-treated cells compared to controls
322 (Supplemental Figure 5C). When we analyzed our live cell imaging experiment to understand
323 the origin of these cells, we found examples of tdTomato^{neg}zsGreen^{+}OLCmarker^{+} cells that
324 arose from a tdTomato^{neg} cell (Supplemental Figure 5D). These tdTomato^{neg} cells did not have
325 OPC morphology 7DPT (Supplemental Figure 1,5D, Supplemental Video 2). Rather, they
326 showed morphologies typical of astrocytes (Supplemental Figure 1,5D, Supplemental Video
327 2), suggesting the conversion of an astrocyte- like Aldh1l1^{neg} cell.
328
329 **Characterization of *Sox10*-mediated DLR using scRNA-seq**
330 Given that *Sox10* increased the number of mOLs from *Aldh1l1* astrocytes (Figure 2D,F), we
331 next probed the mechanisms underlying *Sox10*-mediated reprogramming. We
332 performed scRNA-sequencing at three additional timepoints (D0 prior to transduction,
333 3DPT, and 8DPT) on Cre-control and *Sox10*-treated cultures. For analysis, we combined
334 cells from D0, 3DPT, 8DPT and 14DPT (Supplemental Figure 6B). We excluded cells with
335 microglia and VLMC markers (Supplemental Figure 6C). Clustering analysis of the remaining
336 cells showed the appearance of 10 distinct clusters (Figure 3A). We characterized these
337 clusters based on expression of genes associated with astrocytes, oligodendrocytes, and
338 NG2 cells, as well as proliferation markers (Figure 3B-C).
339
340 First, we examined the molecular identities of cells in our starting cultures. D0 cells were
341 found in clusters 1, 3, 5 and 9 and showed expression of canonical astrocyte markers,
342 including *Slc1a3, Aqp4, Atp1b2, Glul* and *Gfap* (Figure 3B,D). Of interest, clusters 1, 3 and 5
343 showed expression of *Aldh1l1*, but this gene was absent in cluster 9 (Figure 3B), which could
344 explain the conversion of tdTomato^{neg} cells observed in our fate mapping experiments
345 (Supplemental Figure 5). Altogether, this suggests that early postnatal cultures are
346 heterogeneous and comprised of distinct astrocyte-like populations (clusters).
347

To understand the cell fate transitions that occur over the reprogramming timecourse, we performed trajectory analysis with Slingshot (35) (Figure 3E) and Monocle3 (36–40) (Figure 3F). Slingshot and Monocle3 both reconstructed trajectories with clusters 6 and 4 as terminal branches (Figure 3E-F). We then examined the origin of cells comprising each cluster. As expected, the clusters formulating earlier roots of the Monocle3 branches (clusters 0, 1, 3, 9) were primarily comprised of D0, 3DPT, and 8DPT timepoints (Figure 3G). Clusters 6 and 4, were predominantly comprised of 14DPT samples, and in particular, cells from *Sox10*-treated samples (D14_S) (Figure 3G). Analysis of the differentially expressed genes (DEGs) at these branches showed that cluster 6 and branch 14 of the Monocle3 trajectory were enriched in the OLC genes *Sox10* (21–24) (p- and q-value=0), *Bcas1* (45*)* (p- and q-value=0), and *Omg* (46,47) (p- and q-value=0 (Supplemental Figure 7A). In contrast, cluster 4 and the Monocle trajectory branch 11 showed expression of the genes *Lcn2* (p- and q-value=0) and *Igfbp5* (p- and q-value=0), (Supplemental Figure 7B) previously shown to be expressed in reactive astrocytes (48–50). All Monocle3-derived differentially expressed genes can be found in Data S2. Altogether, these analyses suggest that the trajectory to branch 14/cluster 6 represents the path of astrocyte to OLC conversion.

To determine how *Sox10* would influence the gene regulatory network of cells in clusters 6 and 4, we performed *in silico* perturbation of *Sox10* using CellOracle (41). *in silico* knock out (KO) of *Sox10* predicted a large shift away from a cluster 6 identity and little change away from the identity of cluster 4 (Figure 3H). In agreement, *in silico* knock in (KI) of *Sox10* showed a large shift towards a cluster 6 identify and little change towards a cluster 4 identity (Figure 3I). This suggests that leaf 14 and cluster 6 represent cells with a gene regulatory network most affected by *Sox10*.

As cluster 6 was comprised of both *Sox10*-treated and Cre-control cells, we then performed a differential gene expression analysis of 14DPT Cre-control and *Sox10*-treated cells within this cluster. 175 DEGs were found, with the top genes (expressed in at least 50% of Cluster 6, *Sox10*-treated cells and with a difference of at least 0.5 pct between Cre-control and *Sox10*-treated cultures) clustered and provided in a dotplot (Figure 3J). This analysis highlighted that genes including *Omg*, *Bcas1*, *Pdgfra*, *Cldn11 (51)*, and *Sox10* are enriched in *Sox10*-treated cells compared to Cre-control cells, suggesting that *Sox10*-treated cells are more representative of OLCs than the Cre-control cells exposed to OPC and OL media alone.

Understanding the genetic drivers of astrocyte to OLC DLR

Our analysis showed that *Sox10* was important for determining the OLC identity of cluster 6. We specifically chose *Sox10* based on its role in OLC fate specification and development (21–24). To understand whether there might be other [better] candidate genes that would promote an OLC identity, we used an unbiased, deep learning perturbation model, Fatecode (44), to predict genes that would allow cells to shift from a cluster 4 identity (astrocytes at 14DPT, not fully reprogrammed) to a cluster 6 identity (OLCs at 14DPT, end state of DLR). Following training of the Fatecode model on our *Sox10* and Cre-control treated DLR dataset, we identified perturbation on node 16 of the latent layer as one which increased the

392 number of cells in cluster 6 whilst simultaneously reducing the number of cells in clusters
393 0, 2, 4, 5 and 7. (Figure 3K). Given that the total number of cells in the dataset does not
394 change, this suggests that the perturbation on node 16 of the latent layer was pushing cells
395 that did not reprogram (astrocytes at 8 and 14DPT) towards a reprogrammed (OLCs at
396 14DPT) fate. To identify the genes driving this shift,we ranked the absolute value of gene
397 expression changes to obtain a list of 3000 genes involved in this perturbation, with the top
398 40 genes listed in Table S4. Strikingly, we observed that *Sox10* was ranked as the ninth most
399 correlated gene and the top TF driving this shift (Table S4). This supports our previous
400 findings that suggest *Sox10* drives astrocyte to iOLC DLR. Additionally, we observed genes
401 important for myelination (*Plp1, Mbp*) (52), as well as other TFs previously identified with
402 OLC differentiation and myelination (*Sox3* (53)*, Klf9* (54)) as integral to this shift (Table S4).
403 Taken together, these findings further support the importance
404 of *Sox10* in reprogramming astrocytes to iOLCs and identify additional genes and TFs that
405 may be ideal candidates for astrocyte to iOLC reprogramming.
406
407 **DISCUSSION**
408 Here, we show astrocyte to iOLC conversion with *Sox10* or *Olig2* using a battery of
409 experimental tools, including astrocyte fate mapping, live cell imaging, scRNA-
410 seq timecourse and unbiased deep learning. While previous studies demonstrated the
411 generation of iOLCs from different types of somatic cells using combinations
412 of *Sox10*, *Olig2* and *Nkx6.2* (2,3,55), ours is the first to compare the individual
413 reprogramming ability of each these TFs in astrocytes. Using *Aldh1l1*-based fate-mapping,
414 we found that that *Sox10* and *Olig2* convert Aldh1l1$^+$ astrocytes to iOLCs.
415
416 In contrast to *Sox10* and *Olig2*, *Nkx6.2* was unable to convert *Aldh1l1*$^+$astrocytes to new
417 iOLCs. Unlike *Sox10* and *Olig2*, which define oligodendrocyte identity and continue to shape
418 their gene regulatory network throughout life (56), *Nkx6.2* may be unable to direct a stable
419 iOLC identity. In support of this, previous work investigating pericyte to OL reprogramming
420 found that inclusion of *Nkx6.2* in their reprogramming cocktail was refractory to
421 reprogramming (3). In addition to observing the activation of genes unrelated
422 to oligodendrogenesis, genes required for OPC identity were downregulated when cells were
423 transduced with *Nkx6.2* (3).
424
425 In a previous study, Khanghahi *et al*. investigated *Sox10*-mediated astrocyte to OLC
426 conversion. Ectopic expression of *Sox10* in astrocytes *in vitro* led to an increase in OPCs at
427 21DPT (14), a different OLC type and longer time to conversion than we observed in our
428 study. Although similar experimental designs were used in both studies (cortical P3-P5
429 astrocytes cultured in OPC media in Khanghahi *et al*. versus P0-P5 cortical astrocytes
430 cultured in OPC followed by OL media in our study), these discrepancies may be due to the
431 use of different viral delivery strategies and metrics of reprogramming. In our study, we used
432 lentiviral delivery of *Sox10*-P2A-zsGreen under the control of the long
433 (2178bp) hGFAP promoter (57). In addition, we used Ai14;Aldh1l1-CreERT2 mice and
434 quantified only the iOLCs with an astrocyte origin (based
435 on tdTomato$^+$OLC marker$^+$expression). In contrast, in the Khanghahi *et al.* study, the authors

436 used a SFFV promoter to deliver *Sox10*-IRES-GFP and reported the number of GFP+ iOLCs in
437 their *Sox10*-transduced cultures. Without an astrocyte specific promoter and stringent
438 lineage tracking, it is difficult to conclude that iOPCs were the result of astrocyte conversion.
439 A non-specific delivery strategy could instead hit a contaminating, perhaps more distantly
440 related cell that would need more time to convert.
441
442 In this regard, a recent study suggested that the conversion reported in studies of *in*
443 *vivo* astrocyte to neuron DLR (6,58,59) was not true reprogramming, but rather the result of
444 erroneous labelling of endogenous neurons due to technical confounds (27). As a result, the
445 DLR community has advocated for the stringent validation of DLR paradigms. In this study,
446 we first examined astrocyte to iOLC conversion in Ai14 cells. This enabled the permanent
447 labeling of transduced cells and therefore, the tracking of those cells through the
448 DLR timecourse. To then validate our findings, we used Aldh1l1-astrocyte fate mapping,
449 which highlighted a lack of conversion with *Nkx6.2*.
450
451 When performing our lineage tracing experiments, we also discovered a subpopulation of
452 cells (*Aldh1l1*-tdTomato^{neg}zsGreen^{+}OLCmarker^{+}) that was converted by *Sox10* at a high
453 reprogramming efficiency (Supplemental Figure 5C). scRNA-seq analysis of cells prior to
454 conversion also showed a cluster with low *Aldh1l1* expression compared to the other
455 astrocyte clusters, but with similar levels of *Gfap* expression (Figure 3B), which could
456 explain its transduction by the LV-GFAP::*Sox10*. These *Aldh1l1*^{lo}*Gfap*^{hi} cells were
457 predominantly characterized by mature astrocyte markers but also showed expression of
458 genes found in NG2 glia (*Cspg, Pdgfra*) (Figure 3B-C). Curiously, this population did not show
459 expression of proliferation marker *Mki67* (Figure 3C), in contrast to previous studies showing
460 that astrocyte-like NG2 glia are proliferative (60,61). Of interest, one study reported high co-
461 expression of *Gfap*, *Cspg4* and *Pdgfra* in early postnatal astrocytes (62). This leads to the
462 intriguing idea that these cells represent a population of *Aldh1l1*^{lo}expressing astrocytes. If
463 so, *Aldh1l1*-fate-mapping would underestimate reprogramming efficiencies. The presence
464 of these *Aldh11l*^{lo} cells shows that astrocyte cultures are heterogeneous and that different
465 types of astrocytes or astrocyte-like cells may be suitable targets for DLR. Further studies
466 using scRNA barcoding and CellOracle to profile the different types of astrocytes that are
467 amenable to reprogramming will be beneficial in designing more specific and tailored DLR
468 strategies.
469
470 Conversion of *Aldh1l1*^{pos} astrocytes to PDGFRa^{+}tdTomato^{+}zsGreen^{+} iOPCs using *Olig2*
471 occurred at a relatively low rate, with an average conversion efficiency of 16.75% cells. This
472 conversion was even lower for the generation of mature MBP^{+}tdTomato^{+}zsGreen^{+}OLs by
473 *Sox10*, with an average conversion efficiency of 2.83%. This may suggest that
474 although *Sox10* may generate more mature OLCs, it can only do this in a select number of
475 'elite' donor cells. Alternatively, the absence of a substrate to myelinate in our cultures may
476 preclude the true reprogramming ability of *Sox10*. OL survival *in vitro* and *in vivo* has been
477 shown to be dependent on the presence of axons (63). Furthermore, previous studies have
478 shown that mRNA expression of myelin genes is increased when OLs are cultured in the
479 presence of neurons (64), and differentiation of OPCs can be induced with bead or nanofiber

480 scaffolding (65,66). However, additional factors, or the discovery of "better" TFs
481 may also allow for increased reprogramming efficiency. It remains to be determined whether
482 the genes predicted by Fatecode in this study will improve the efficiencies of OLC
483 generation. Nonetheless, it is important to note that the extent of iOLC generation must be
484 balanced with the extent of astrocyte loss as many studies have shown that widespread loss
485 of astrocytes can be detrimental (67,68).
486
487 Investigation of the reprogramming trajectory of *Sox10* and Cre-control treated cells showed
488 a bifurcation, where the cells either converted to iOLCs or remained as astrocytes (Figure
489 3F). It remains to be determined if this is a genetic hurdle or a metabolic hurdle, similar to
490 studies of astrocyte to neuron conversion (69). Future studies investigating the genes that
491 characterize the 'tipping point' of conversion will be useful in identifying the mechanisms of
492 astrocyte to iOLC reprogramming. A clearer understanding of how different astrocyte types
493 convert to iOLCs and the mechanisms that underly the reprogramming processes will help
494 us identify the best DLR paradigm for therapeutic applications.
495
496 **ACKNOWLEDGMENTS**
497 The authors are grateful to Dr. Lindsey Fiddes at the Microscope Imaging Facility for
498 assistance with live cell imaging. Next-generation sequencing was performed at the
499 Donnelly
500 Sequencing Facility. J.B. was supported by the Baden Havard Endowment Fund, the Ontario
501 Graduate Scholarship and the MITACs Accelerate Fellowship. This work was supported by
502 grants to M.F. from CIHR (PJT-175254), Medicine by Design (Cycle 2
503 Funding), Temerty Foundation (Pathway Grant), Ontario Institute of Regenerative Medicine
504 (Kickstart Innovation Investment Program), the Stem Cell Network (Early Career Researcher
505 Jump Start Award), the Connaught Foundation (Innovation Grant), CFA-JELF program for
506 microscopy infrastructure, and to S.A.Y. from the CFI-JELF program for scRNA-seq related
507 infrastructure.
508
509 **DATA AVAILABILITY**
510 RNA sequence data is deposited in GEO (accession number
511 GSE263185). Genetables are provided as a Cyvers link through the Github page (see
512 methods) housing the scripts used in the manuscript.
513
514 **AUTHOR CONTRIBUTIONS**
515 Conceptualization, M.F.; Methodology, J.B., G.D.B., M.F.; Software, E.Y.S., M.S.; Formal
516 Analysis, J.B., E.Y.S., M.S., S.A.Y., M.F.; Investigation, J.B., E.Y.S., A.O., M.S., K.L., M. Fahim,
517 H.T.T., D.L.C., A.D., and S.A.Y.; Writing – Original Draft, J.B. and E.Y.S.; Writing – Review and
518 Editing, M.F.; Visualization, J.B., E.Y.S., M.S.; Supervision, G.D.B., M.F.; Funding
519 Acquisition, S.A.Y., M.F.
520
521 **COMPETING INTERESTS**

522 MF, JB are co-inventors on a patent application (Applicants: Justine Bajohr,
523 Maryam Faiz, The governing council of the University of Toronto; Inventors: Maryam Faiz,
524 Justine Bajohr, US Provisional Filed #63/497,357, April 20, 2023).
525
526 **FIGURE LEGENDS**
527
528 **Figure 1. *Sox10*, *Olig2* and *Nkx6.2* convert GFAP+ cells to oligodendrocyte lineage**
529 **cells. (A)** Experimental design and timeline. **(B)** Quantification of PDGFRα$^+$tdTomato$^+$iOPCs,
530 O4$^+$tdTomato$^+$ iCOPs and MBP$^+$tdTomato$^+$ iOLs at 8 (n=5), 10 (n=4), 12 (n=5) and 14 (n=7)
531 days post transduction (DPT). Data are presented as mean ± SEM, each data point
532 represents one individual cell culture experiment; at each time point and for each cell type
533 marker, a matched pairs one-way ANOVA or Kruskal-Wallis (d8, d10, d12) or one- way ANOVA
534 (d14) was performed with Dunnet's post testing (*= p<0.05, *** = p<
535 0.001). **(C)** Representative images of PDGFRα$^+$tdTomato$^+$,O4$^+$tdTomato$^+$ and
536 MBP$^+$tdTomato$^+$ cells at 12DPT. Single channel images are shown of the boxed cells (arrows
537 indicate double positive cells). Scale bar = 50um. **(D)** UMAP clustering of *Olig2-*, *Sox10-*
538 , *Nkx6.2-* and control (Cre) transduced cells at 14DPT **(E)** UMAP of (D) overlayed with
539 treatment (*Olig2-*, *Sox10-*, *Nkx6.2-* and control (Cre)) **(F)** Proportion analysis of clusters
540 found in *Olig2-*, *Sox10-*, *Nkx6.2-*, and control (Cre) transduced cells. **(G)** Heatmap of top
541 upregulated genes from each cluster in (D).
542
543 **Figure 2. Lineage tracing confirms true conversion of astrocytes to oligodendrocyte**
544 **lineage cells.**
545 **(A)** Experimental design, timeline and outcomes. **(B)** Quantification
546 of tdTomato$^+$zsGreen$^+$PDGFRα$^+$ iOPCs at 12DPT (n= 3). Data are presented as mean ± SEM,
547 each data point represents one individual cell culture, a paired t-test was performed (** =
548 p<0.01). **(C)** Quantification of tdTomato$^+$zsGreen$^+$O4$^+$ iCOPs at 14DPT (n = 4). Data
549 are presented as mean ± SEM, each data point represents one individual cell
550 culture, a Wilcoxon test was performed (ns). **(D)** Quantification
551 of tdTomato$^+$zsGreen$^+$MBP$^+$ iOLs at 12DPT (n= 4 for *Sox10, Nkx6.2*, n= 3 for *Cre*). Data are
552 presented as mean ± SEM, each data point represents one individual cell culture, a one-way
553 ANOVA with Dunnet's post testing was performed (* = p<0.05). **(E)** Representative image of
554 PDGFRα$^+$tdTomato$^+$zsGreen$^+$ cells 12DPT. Single channel images are shown of the boxed
555 cells (arrows indicate triple positive cells, scale bar = 50um (merge) and 20um (single
556 channel)). **(F)** Representative image of MBP$^+$tdTomato$^+$zsGreen$^+$ cells 12DPT. Single channel
557 images are shown of the boxed cells (arrows indicate triple positive cells, scale bar = 50um
558 (merge) and 20um (single channel)). **(G)** Representative tdTomato$^+$zsGreen$^+$ cell with
559 astrocyte-like morphology at onset (7DPT) and OLC expression at the end (12DPT) of live cell
560 tracking (arrow indicates tracked cell, scale bar = 50um).
561
562 **Figure 3. Characterization of DLR using scRNA-seq shows terminal oligodendrocyte**
563 **cluster of cells at day 14 driven by *Sox10*. (A)** UMAP clustering
564 of *Sox10* and *Cre* control treated cells from prior to transduction, as well as 3, 8 and
565 14DPT **(B)** Canonical astrocyte gene expression (log-normalized, y-axis) separated by

cluster (x-axis) and coloured by timepoint and treatment group. **(C)** Canonical gene expression (log-normalized, y-axis) of NG2 glia, VLMC, OLC, microglia and proliferation, separated by cluster (x-axis) and coloured by timepoint and treatment group. **(D)** UMAP clustering from (A) overlayed with timepoint and treatment group **(E)** Slingshot lineage analysis of *Sox10* and *Cre* control treated clusters overlaid with UMAP embeddings. **(F)** Monocle3 lineage analysis of *Sox10* and *Cre* control treated clusters overlaid on UMAP plot and coloured by pseudotime predictions. **(G)** The number of cells (y-axis) per cluster (x-axis) originating from each of the coloured timepoint+treatmentgroups. **(H)** CellOracle modeling of *in silico Sox10* knock out (KO) overlaid onto UMAP plot. Arrows indicate trajectory prediction with *Sox10* KO. **(I)** CellOracle modeling of *in silico Sox10* knock in (KI) overlaid onto UMAP plot. Arrows indicate trajectory prediction with *Sox10* KI **(J)** Clustered, top differentially expressed genes (dots, y-axis) between 14DPT *Sox10 (D14_S,* Beige, left*)* and *Cre (D14_C,* Blue, right*)* control treated cells from cluster 6. Size of dot is scaled to percent of cells in the cluster expressing that gene, colour of dot represents the average scaled expression of the gene across cells. **(K)** Predicted cell types following Fatecode perturbation on node 16 of the latent layer in the *Sox10* and control treated dataset. Blue represents the number of cells prior to perturbation. Orange (overlayed) represents the number of cells following perturbation.

REFERENCES

1. Bajohr J, Faiz M. Direct Lineage Reprogramming in the CNS. In: Turksen K, editor. Cell Biology and Translational Medicine, Volume 6: Stem Cells: Their Heterogeneity, Niche and Regenerative Potential [Internet]. Cham: Springer International Publishing; 2020 [cited 2024 Mar 15]. p. 31–48. Available from: https://doi.org/10.1007/5584_2019_374

2. Najm FJ, Lager AM, Zaremba A, Wyatt K, Caprariello AV, Factor DC, et al. Transcription factor–mediated reprogramming of fibroblasts to expandable, myelinogenic oligodendrocyte progenitor cells. Nat Biotechnol. 2013 May;31(5):426–33.

3. Kim KP, Li C, Bunina D, Jeong HW, Ghelman J, Yoon J, et al. Donor cell memory confers a metastable state of directly converted cells. Cell Stem Cell. 2021 Jul 1;28(7):1291-1306.e10.

4. Heinrich C, Blum R, Gascón S, Masserdotti G, Tripathi P, Sánchez R, et al. Directing astroglia from the cerebral cortex into subtype specific functional neurons. PLoS Biol. 2010 May 18;8(5):e1000373.

5. Heins N, Malatesta P, Cecconi F, Nakafuku M, Tucker KL, Hack MA, et al. Glial cells generate neurons: the role of the transcription factor Pax6. Nat Neurosci. 2002 Apr;5(4):308–15.

604 6. Guo Z, Zhang L, Wu Z, Chen Y, Wang F, Chen G. In vivo direct reprogramming of reactive
605 glial cells into functional neurons after brain injury and in an Alzheimer's disease
606 model. Cell Stem Cell. 2014 Feb 6;14(2):188–202.

607 7. Liu Y, Miao Q, Yuan J, Han S, Zhang P, Li S, et al. Ascl1 Converts Dorsal Midbrain
608 Astrocytes into Functional Neurons In Vivo. J Neurosci. 2015 Jun 24;35(25):9336–55.

609 8. Levison SW, Goldman JE. Both oligodendrocytes and astrocytes develop from
610 progenitors in the subventricular zone of postnatal rat forebrain. Neuron. 1993
611 Feb;10(2):201–12.

612 9. Kriegstein A, Alvarez-Buylla A. The glial nature of embryonic and adult neural stem
613 cells. Annu Rev Neurosci. 2009;32:149–84.

614 10. Masserdotti G, Gascón S, Götz M. Direct neuronal reprogramming: learning from and
615 for development. Development. 2016 Jul 15;143(14):2494–510.

616 11. Hörmanseder E. Epigenetic memory in reprogramming. Current Opinion in Genetics &
617 Development. 2021 Oct 1;70:24–31.

618 12. Bussmann LH, Schubert A, Manh TPV, Andres LD, Desbordes SC, Parra M, et al. A
619 Robust and Highly Efficient Immune Cell Reprogramming System. Cell Stem Cell. 2009
620 Nov 6;5(5):554–66.

621 13. Xie H, Ye M, Feng R, Graf T. Stepwise reprogramming of B cells into macrophages. Cell.
622 2004 May 28;117(5):663–76.

623 14. Mokhtarzadeh Khanghahi A, Satarian L, Deng W, Baharvand H, Javan M. In vivo
624 conversion of astrocytes into oligodendrocyte lineage cells with transcription factor
625 Sox10; Promise for myelin repair in multiple sclerosis. PLoS One. 2018 Sep
626 13;13(9):e0203785.

627 15. Marques S, Zeisel A, Codeluppi S, van Bruggen D, Mendanha Falcão A, Xiao L, et al.
628 Oligodendrocyte heterogeneity in the mouse juvenile and adult central nervous system.
629 Science. 2016 Jun 10;352(6291):1326–9.

630 16. Zhou Q, Wang S, Anderson DJ. Identification of a novel family of oligodendrocyte
631 lineage-specific basic helix-loop-helix transcription factors. Neuron. 2000
632 Feb;25(2):331–43.

633 17. Wang H, Xu L, Lai C, Hou K, Chen J, Guo Y, et al. Region-specific distribution of Olig2-
634 expressing astrocytes in adult mouse brain and spinal cord. Molecular Brain. 2021 Feb
635 17;14(1):36.

636 18. Buffo A, Vosko MR, Ertürk D, Hamann GF, Jucker M, Rowitch D, et al. Expression pattern
637 of the transcription factor Olig2 in response to brain injuries: Implications for neuronal
638 repair. Proc Natl Acad Sci U S A. 2005 Dec 13;102(50):18183–8.

639 19. Marshall CAG, Novitch BG, Goldman JE. Olig2 directs astrocyte and oligodendrocyte
640 formation in postnatal subventricular zone cells. J Neurosci. 2005 Aug 10;25(32):7289–
641 98.

642 20. Tatsumi K, Isonishi A, Yamasaki M, Kawabe Y, Morita-Takemura S, Nakahara K, et al.
643 Olig2-Lineage Astrocytes: A Distinct Subtype of Astrocytes That Differs from GFAP
644 Astrocytes. Front Neuroanat. 2018;12:8.

645 21. Liu Z, Hu X, Cai J, Liu B, Peng X, Wegner M, et al. Induction of oligodendrocyte
646 differentiation by Olig2 and Sox10: evidence for reciprocal interactions and dosage-
647 dependent mechanisms. Dev Biol. 2007 Feb 15;302(2):683–93.

648 22. Pozniak CD, Langseth AJ, Dijkgraaf GJP, Choe Y, Werb Z, Pleasure SJ. Sox10 directs
649 neural stem cells toward the oligodendrocyte lineage by decreasing Suppressor of
650 Fused expression. Proc Natl Acad Sci U S A. 2010 Dec 14;107(50):21795–800.

651 23. Takada N, Kucenas S, Appel B. Sox10 is necessary for oligodendrocyte survival
652 following axon wrapping. Glia. 2010 Jun;58(8):996–1006.

653 24. Stolt CC, Rehberg S, Ader M, Lommes P, Riethmacher D, Schachner M, et al. Terminal
654 differentiation of myelin-forming oligodendrocytes depends on the transcription factor
655 Sox10. Genes Dev. 2002 Jan 15;16(2):165–70.

656 25. Awatramani R, Scherer S, Grinspan J, Collarini E, Skoff R, O'Hagan D, et al. Evidence
657 That the Homeodomain Protein Gtx Is Involved in the Regulation of Oligodendrocyte
658 Myelination. J Neurosci. 1997 Sep 1;17(17):6657–68.

659 26. Cai J, Zhu Q, Zheng K, Li H, Qi Y, Cao Q, et al. Co-localization of Nkx6.2 and Nkx2.2
660 Homeodomain Proteins in Differentiated Myelinating Oligodendrocytes. Glia. 2010
661 Mar;58(4):458–68.

662 27. Wang LL, Serrano C, Zhong X, Ma S, Zou Y, Zhang CL. Revisiting astrocyte to neuron
663 conversion with lineage tracing in vivo. Cell. 2021 Oct 14;184(21):5465-5481.e16.

664 28. McCarthy KD, de Vellis J. Preparation of separate astroglial and oligodendroglial cell
665 cultures from rat cerebral tissue. J Cell Biol. 1980 Jun;85(3):890–902.

666 29. Bray NL, Pimentel H, Melsted P, Pachter L. Near-optimal probabilistic RNA-seq
667 quantification. Nat Biotechnol. 2016 May;34(5):525–7.

30. Melsted P, Booeshaghi AS, Liu L, Gao F, Lu L, Min KH (Joseph), et al. Modular, efficient and constant-memory single-cell RNA-seq preprocessing. Nat Biotechnol. 2021 Jul;39(7):813–8.

31. Hao Y, Hao S, Andersen-Nissen E, Mauck WM, Zheng S, Butler A, et al. Integrated analysis of multimodal single-cell data. Cell. 2021 Jun 24;184(13):3573-3587.e29.

32. Gu Z, Eils R, Schlesner M. Complex heatmaps reveal patterns and correlations in multidimensional genomic data. Bioinformatics. 2016 Sep 15;32(18):2847–9.

33. Dugas JC, Tai YC, Speed TP, Ngai J, Barres BA. Functional genomic analysis of oligodendrocyte differentiation. J Neurosci. 2006 Oct 25;26(43):10967–83.

34. Marsh S. scCustomize:Custom Visualizations & Functions for Streamlined Analyses of Single Cell Sequencing. [Internet]. 2021. Available from: https://doi.org/10.5281/zenodo.5706430

35. Street K, Risso D, Fletcher RB, Das D, Ngai J, Yosef N, et al. Slingshot: cell lineage and pseudotime inference for single-cell transcriptomics. BMC Genomics. 2018 Jun 19;19(1):477.

36. Trapnell C, Cacchiarelli D, Grimsby J, Pokharel P, Li S, Morse M, et al. The dynamics and regulators of cell fate decisions are revealed by pseudotemporal ordering of single cells. Nat Biotechnol. 2014 Apr;32(4):381–6.

37. Qiu X, Mao Q, Tang Y, Wang L, Chawla R, Pliner HA, et al. Reversed graph embedding resolves complex single-cell trajectories. Nat Methods. 2017 Oct;14(10):979–82.

38. Cao J, Spielmann M, Qiu X, Huang X, Ibrahim DM, Hill AJ, et al. The single cell transcriptional landscape of mammalian organogenesis. Nature. 2019 Feb;566(7745):496–502.

39. Traag VA, Waltman L, van Eck NJ. From Louvain to Leiden: guaranteeing well-connected communities. Sci Rep. 2019 Mar 26;9(1):5233.

40. Levine JH, Simonds EF, Bendall SC, Davis KL, Amir E ad D, Tadmor M, et al. Data-driven phenotypic dissection of AML reveals progenitor-like cells that correlate with prognosis. Cell. 2015 Jul 2;162(1):184–97.

41. Kamimoto K, Stringa B, Hoffmann CM, Jindal K, Solnica-Krezel L, Morris SA. Dissecting cell identity via network inference and in silico gene perturbation. Nature. 2023 Feb;614(7949):742–51.

42. Wickham H. ggplot2: Elegant Graphics for Data Analysis [Internet]. New York, NY: Springer; 2009 [cited 2024 Mar 16]. Available from: https://link.springer.com/10.1007/978-0-387-98141-3

43. RStudio: Integrated Development for R [Internet]. 2020. Available from: http://www.rstudio.com/

44. Sadria M, Layton A, Goyal S, Bader GD. Fatecode: Cell fate regulator prediction using classification autoencoder perturbation [Internet]. bioRxiv; 2022 [cited 2024 Mar 15]. p. 2022.12.16.520772. Available from: https://www.biorxiv.org/content/10.1101/2022.12.16.520772v1

45. Fard MK, van der Meer F, Sánchez P, Cantuti-Castelvetri L, Mandad S, Jäkel S, et al. BCAS1 expression defines a population of early myelinating oligodendrocytes in multiple sclerosis lesions. Sci Transl Med. 2017 Dec 6;9(419):eaam7816.

46. Vourc'h P, Andres C. Oligodendrocyte myelin glycoprotein (OMgp): evolution, structure and function. Brain Res Brain Res Rev. 2004 May;45(2):115–24.

47. Mikol DD, Stefansson K. A phosphatidylinositol-linked peanut agglutinin-binding glycoprotein in central nervous system myelin and on oligodendrocytes. J Cell Biol. 1988 Apr 1;106(4):1273–9.

48. Bi F, Huang C, Tong J, Qiu G, Huang B, Wu Q, et al. Reactive astrocytes secrete lcn2 to promote neuron death. Proceedings of the National Academy of Sciences. 2013 Mar 5;110(10):4069–74.

49. Liddelow SA, Guttenplan KA, Clarke LE, Bennett FC, Bohlen CJ, Schirmer L, et al. Neurotoxic reactive astrocytes are induced by activated microglia. Nature. 2017 Jan 26;541(7638):481–7.

50. Lee WH, Wang GM, Seaman LB, Vannucci SJ. Coordinate IGF-I and IGFBP5 Gene Expression in Perinatal Rat Brain after Hypoxia-Ischemia. J Cereb Blood Flow Metab. 1996 Mar 1;16(2):227–36.

51. Morita K, Sasaki H, Fujimoto K, Furuse M, Tsukita S. Claudin-11/OSP-based Tight Junctions of Myelin Sheaths in Brain and Sertoli Cells in Testis. J Cell Biol. 1999 May 3;145(3):579–88.

52. Kister A, Kister I. Overview of myelin, major myelin lipids, and myelin-associated proteins. Front Chem [Internet]. 2023 Feb 21 [cited 2024 Mar 17];10. Available from: https://www.frontiersin.org/articles/10.3389/fchem.2022.1041961

53. Hoffmann SA, Hos D, Küspert M, Lang RA, Lovell-Badge R, Wegner M, et al. Stem cell factor Sox2 and its close relative Sox3 have differentiation functions in oligodendrocytes. Development. 2014 Jan 1;141(1):39–50.

54. Dugas JC, Ibrahim A, Barres BA. The T3-induced gene KLF9 regulates oligodendrocyte differentiation and myelin regeneration. Mol Cell Neurosci. 2012 May;50(1):45–57.

736 55. Yang N, Zuchero JB, Ahlenius H, Marro S, Ng YH, Vierbuchen T, et al. Generation of
737 oligodendroglial cells by direct lineage conversion. Nat Biotechnol. 2013
738 May;31(5):434–9.

739 56. Sock E, Wegner M. Using the lineage determinants Olig2 and Sox10 to explore
740 transcriptional regulation of oligodendrocyte development. Dev Neurobiol. 2021
741 Oct;81(7):892–901.

742 57. Lee Y, Messing A, Su M, Brenner M. GFAP promoter elements required for region-
743 specific and astrocyte-specific expression. Glia. 2008;56(5):481–93.

744 58. Chen YC, Ma NX, Pei ZF, Wu Z, Do-Monte FH, Keefe S, et al. A NeuroD1 AAV-Based Gene
745 Therapy for Functional Brain Repair after Ischemic Injury through In Vivo Astrocyte-to-
746 Neuron Conversion. Molecular Therapy. 2020 Jan 8;28(1):217–34.

747 59. Qian H, Kang X, Hu J, Zhang D, Liang Z, Meng F, et al. Reversing a model of Parkinson's
748 disease with in situ converted nigral neurons. Nature. 2020 Jun;582(7813):550–6.

749 60. Janeckova L, Knotek T, Kriska J, Hermanova Z, Kirdajova D, Kubovciak J, et al. Astrocyte-
750 like subpopulation of NG2 glia in the adult mouse cortex exhibits characteristics of
751 neural progenitor cells. Glia. 2024;72(2):245–73.

752 61. Kirdajova D, Valihrach L, Valny M, Kriska J, Krocianova D, Benesova S, et al. Transient
753 astrocyte-like NG2 glia subpopulation emerges solely following permanent brain
754 ischemia. Glia. 2021 Nov;69(11):2658–81.

755 62. Rusnakova V, Honsa P, Dzamba D, Ståhlberg A, Kubista M, Anderova M. Heterogeneity
756 of Astrocytes: From Development to Injury – Single Cell Gene Expression. PLOS ONE.
757 2013 Aug 5;8(8):e69734.

758 63. Barres BA, Jacobson MD, Schmid R, Sendtner M, Raff MC. Does oligodendrocyte
759 survival depend on axons? Current Biology. 1993 Aug;3(8):489–97.

760 64. Macklin W b., Weill C l., Deininger P l. Expression of myelin proteolipid and basic
761 protein mRNAS in cultured cells. Journal of Neuroscience Research. 1986;16(1):203–
762 17.

763 65. Rosenberg SS, Kelland EE, Tokar E, De La Torre AR, Chan JR. The geometric and spatial
764 constraints of the microenvironment induce oligodendrocyte differentiation. Proc Natl
765 Acad Sci U S A. 2008 Sep 23;105(38):14662–7.

766 66. Lee S, Leach MK, Redmond SA, Chong SYC, Mellon SH, Tuck SJ, et al. A culture system
767 to study oligodendrocyte myelination-processes using engineered nanofibers. Nat
768 Methods. 2012 Sep;9(9):917–22.

67. Bush TG, Puvanachandra N, Horner CH, Polito A, Ostenfeld T, Svendsen CN, et al. Leukocyte infiltration, neuronal degeneration, and neurite outgrowth after ablation of scar-forming, reactive astrocytes in adult transgenic mice. Neuron. 1999 Jun;23(2):297–308.

68. Davis N, Mota BC, Stead L, Palmer EOC, Lombardero L, Rodríguez-Puertas R, et al. Pharmacological ablation of astrocytes reduces Aβ degradation and synaptic connectivity in an ex vivo model of Alzheimer's disease. J Neuroinflammation. 2021 Mar 17;18:73.

69. Gascón S, Masserdotti G, Russo GL, Götz M. Direct Neuronal Reprogramming: Achievements, Hurdles, and New Roads to Success. Cell Stem Cell. 2017 Jul 6;21(1):18–34.

SUPPLEMENTARY INFORMATION

Supplemental Figure 1. Morphological characterization of astrocytes and oligodendrocyte progenitor cells. Quantification of the **(A)** cell length, **(B)** nucleus size, **(C)** number of branches, and **(D)** branch thickness in Aldh1l1+tdTomato+ and PDGFRα+ OPCs (n= 70 per cell, data are presented as mean ± SEM, each data point represents one individual cell , significance was calculated using Welch's t-test (A), Mann Whitney test (B,C) and Kruskal Wallis one-way ANOVA (D), ** = $p<0.01$, **** = $p<0.0001$)

Supplemental Figure 2. 14DPT scRNA-seq processing for initial UMAP generation. (A) Distribution of genes (nFeature), reads (nCount) and percent of mitochondrial reads (percent.mt) per sample. **(B)** UMAP clustering prior to removal of microglia cluster. **(C)**Top upregulated genes characterizing each cluster observed in (B).

Supplemental Figure 3. Characterization of DLR cultures. (A) Quantification of contaminating iOLCs in post-natal astrocyte cultures 3DPT. **(B)** Quantification of MBP expression in tdTomato$^+$ transduced cells 22DPT (n=3, data are presented as mean ± SEM, each data point represents one individual cell culture, a matched pairs one way ANOVA was performed (ns)).

Supplemental Figure 4. Comparison of DLR clusters 14DPT to established datasets of OLCs. (A) Violin plots of cell types annotated by Marques *et al*. 2016 within each cluster (OPC = oligodendrocyte progenitor cells, COPs = committed oligodendrocyte progenitors, NFOL = newly formed oligodendrocyte, MFOL = myelin forming oligodendrocyte, mOL = mature oligodendrocyte).**(B)** Violin plots of cell types annotated by Dugas *et al*. 2006 within each cluster (OL = oligodendrocyte, OPC = oligodendrocyte progenitor cells).

Supplemental Figure 5. Characterization of *Aldh1l1*^{neg} and zsGreen^{neg} iOLCs **(A)** Quantification of (i) tdTomato^{+} and (ii) zsGreen^{+} PDGFRα^{+}iOPCs at 12DPT (n= 3). Data are presented as mean ± SEM, each data point represents one individual cell culture, a paired t-test for (i) and a Wilcoxon test for (ii) was performed. **(B)** Quantification of (i) tdTomato^{+} and (ii) zsGreen^{+} O4^{+}iCOPs at 14DPT (n = 4). Data are presented as mean ± SEM, each data point represents one individual cell culture, a paired t-test was used. **(C)** Quantification of (i) tdTomato^{+} (ii) zsGreen^{+} MBP^{+} OLs at 12DPT (n= 3). Data are presented as mean ± SEM, each data point represents one individual cell culture, a matched pairs one way ANOVA with Geisser –Greenhouse correction and Dunnet's post testing was used (* = $p<0.05$). **(D)** Representative tdTomato^{neg}zsGreen^{+} cell with astrocyte-like morphology at onset (7DPT) and OLC expression at the end (12DPT) of live cell tracking (arrow indicated tracked cell, scale bar = 50um).

Supplemental Figure 6. DLR timecourse scRNA-seq processing for initial UMAP generation. **(A)** Distribution of genes (nFeature), reads (nCount) and percent of mitochondrial reads (percent.mt) per sample. **(B)** UMAP clustering prior to removal of microglia and VLMC clusters. **(C)** Top upregulated genes characterizing each cluster observed in (B).

Supplemental Figure 7. Differential gene expression of clusters in the Monocle3 trajectory. **(A)** Genes enriched in leaf 14 of Monocle3 trajectory. Cells in UMAP colored according to log-normalized gene expression values. **(B)** Genes enriched in leaf 11 of Monocle3 trajectory. Cells in UMAP colored according to log-normalized gene expression values.

Video S1. Live cell conversion of tdTomato^{+}zsGreen^{+} astrocyte to iOLC
Video S2. Live cell conversion of tdTomato^{neg}zsGreen^{+} astrocyte to iOLC
Table S1. Astrocyte and oligodendrocyte progenitor morphology characterization
Table S2. 14DPT scRNA seq cell collection metrics
Table S3. Pre-transduction, 3 and 8DPT scRNA seq cell collection metrics
Table S4. Top 40 genes associated with Fatecode perturbation on node 16 of the latent layer
Data S1. BD Rhapsody Whole Transcriptome Analysis whitelist
Data S2. Monocle3-derived differentially expressed genes

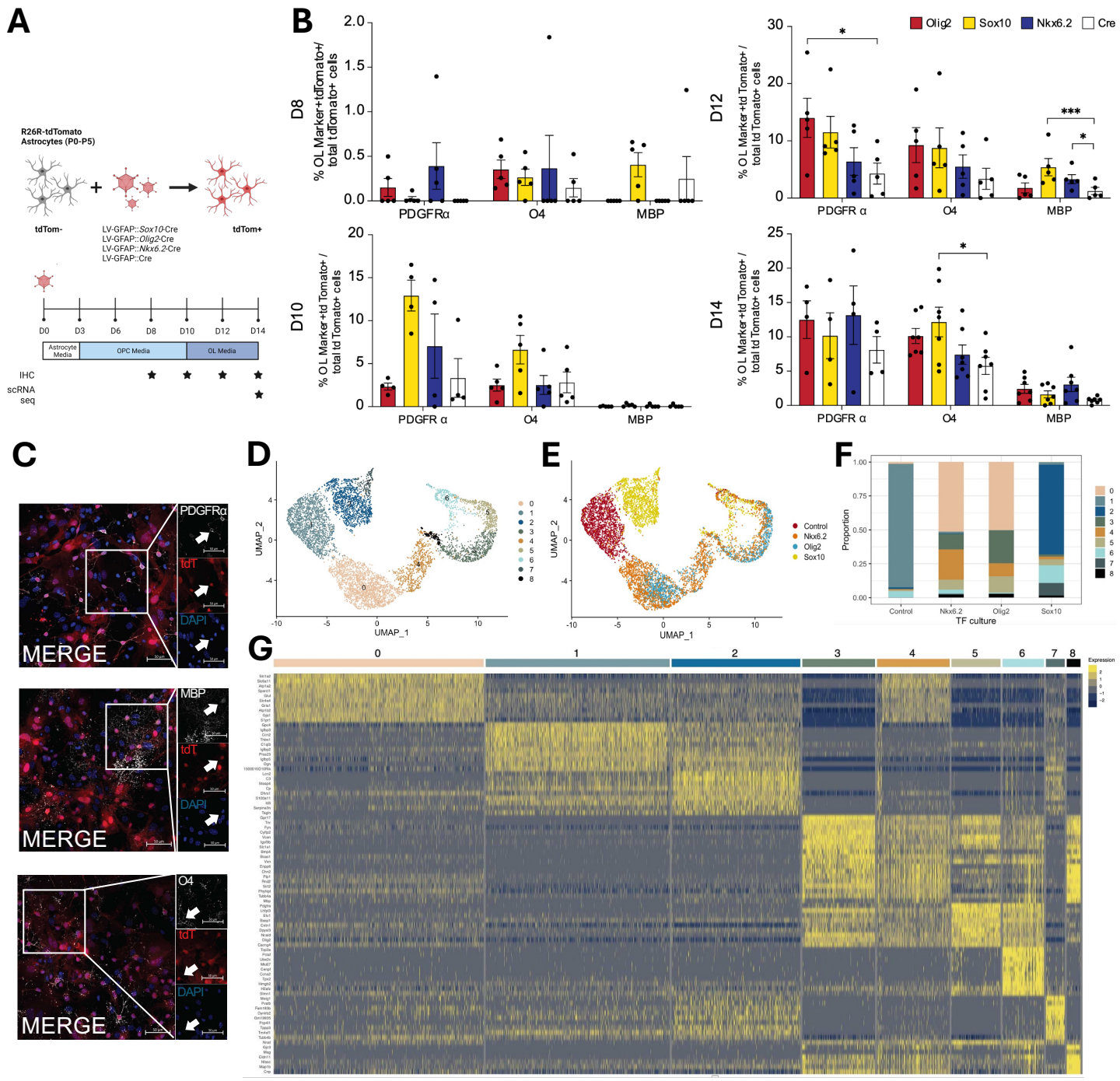
A
R26R-tdTomato
Astrocytes (P0-P5)
tdTom-
LV-GFAP::Sox10-Cre
LV-GFAP::Olig2-Cre
LV-GFAP::Nkx6.2-Cre
LV-GFAP::Cre
tdTom+
D0
D3
D6
D8
D10
D12
D14
Astrocyte Media
OPC Media
OL Media
IHC
scRNA seq
B
D8
D10
D12
D14
% OL Marker+tdTomato+/ total tdTomato+ cells
% OL Marker+td Tomato+ / total td Tomato+ cells
PDGFRα
O4
MBP
Olig2
Sox10
Nkx6.2
Cre
C
PDGFRα
tdT
DAPI
MERGE
MBP
O4
D
UMAP_1
UMAP_2
E
Control
Nkx6.2
Olig2
Sox10
F
Proportion
TF culture
G
Expression

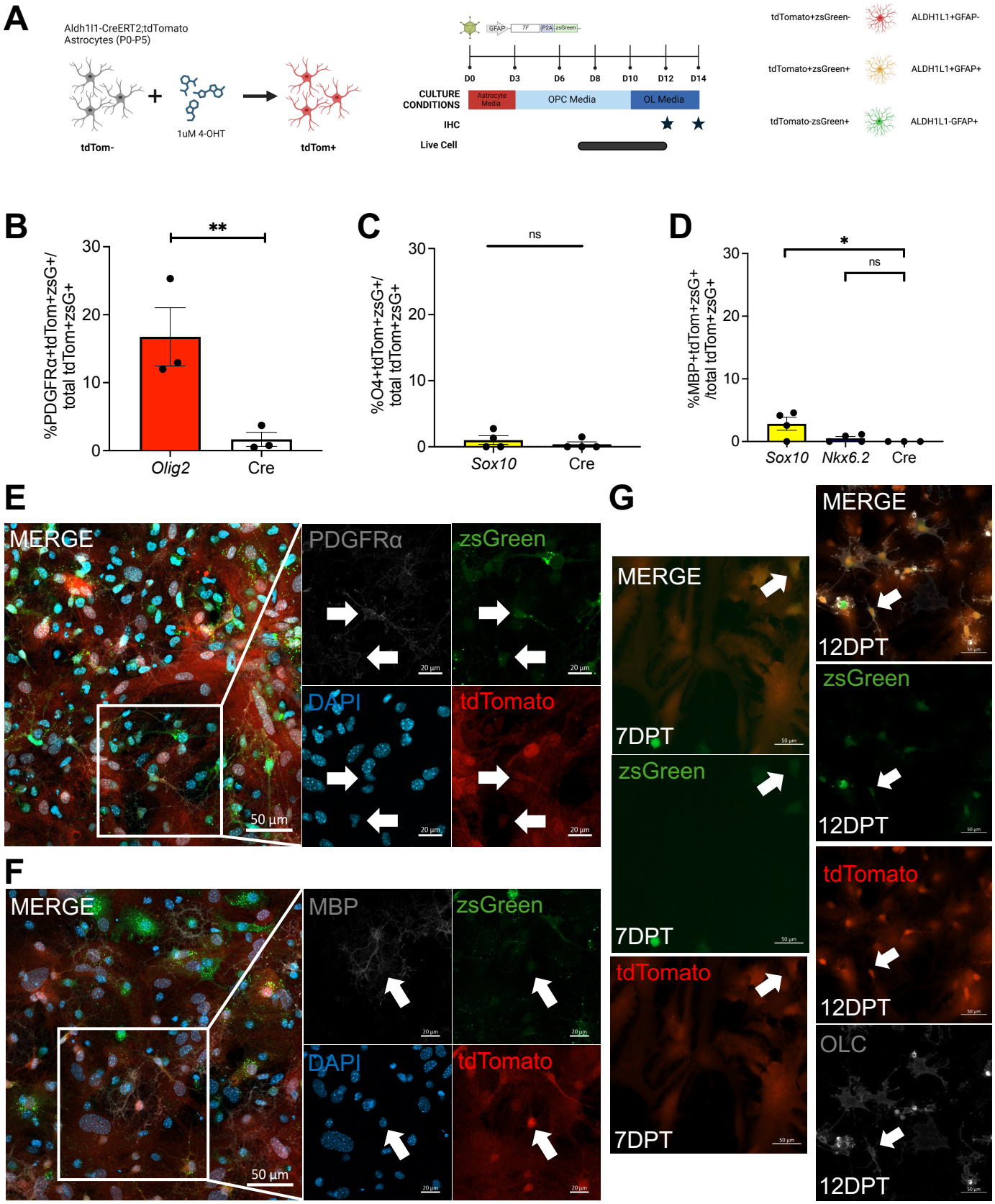
A
Aldh1l1-CreERT2;tdTomato
Astrocytes (P0-P5)
tdTom-
1uM 4-OHT
tdTom+
GFAP
TF
P2A
zsGreen
D0
D3
D6
D8
D10
D12
D14
CULTURE CONDITIONS
Astrocyte Media
OPC Media
OL Media
IHC
Live Cell
tdTomato+zsGreen-
ALDH1L1+GFAP-
tdTomato+zsGreen+
ALDH1L1+GFAP+
tdTomato-zsGreen+
ALDH1L1-GFAP+
B
%PDGFRα+tdTom+zsG+/ total tdTom+zsG+
**
Olig2
Cre
C
%O4+tdTom+zsG+/ total tdTom+zsG+
ns
Sox10
Cre
D
%MBP+tdTom+zsG+ /total tdTom+zsG+
*
ns
Sox10
Nkx6.2
Cre
E
MERGE
PDGFRα
zsGreen
DAPI
tdTomato
50 µm
20 µm
F
MERGE
MBP
zsGreen
DAPI
tdTomato
50 µm
20 µm
G
MERGE
7DPT
zsGreen
7DPT
tdTomato
7DPT
MERGE
12DPT
zsGreen
12DPT
tdTomato
12DPT
OLC
12DPT
50 µm

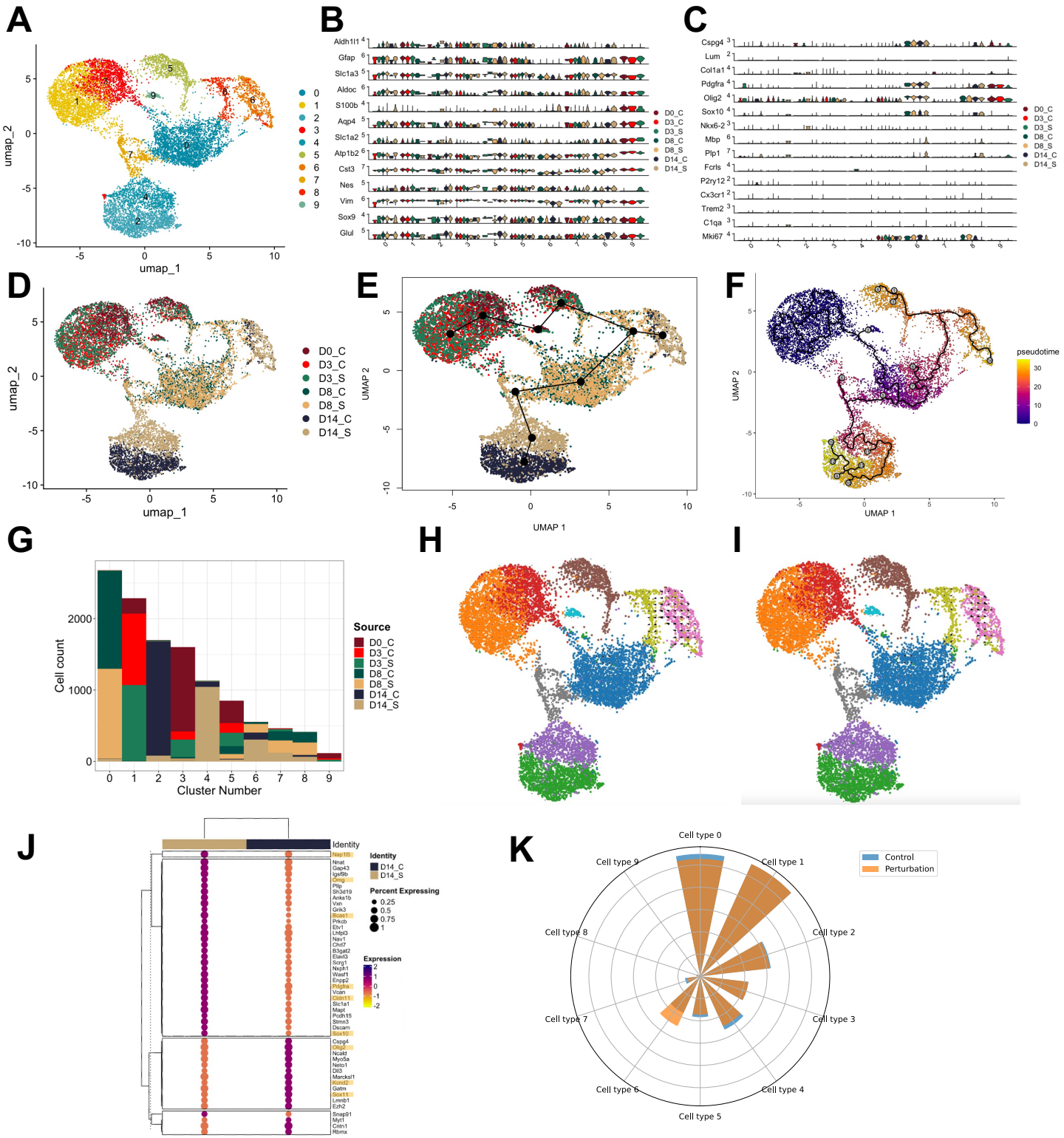
A
umap_1
umap_2
0
1
2
3
4
5
6
7
8
9
B
Aldh1l1
Gfap
Slc1a3
Aldoc
S100b
Aqp4
Slc1a2
Atp1b2
Cst3
Nes
Vim
Sox9
Glul
D0_C
D3_C
D3_S
D8_C
D8_S
D14_C
D14_S
C
Cspg4
Lum
Col1a1
Pdgfra
Olig2
Sox10
Nkx6-2
Mbp
Plp1
Fcrls
P2ry12
Cx3cr1
Trem2
C1qa
Mki67
D
E
UMAP 1
UMAP 2
F
pseudotime
G
Cell count
Cluster Number
Source
H
I
J
Identity
Percent Expressing
Expression
K
Cell type 0
Cell type 1
Cell type 2
Cell type 3
Cell type 4
Cell type 5
Cell type 6
Cell type 7
Cell type 8
Cell type 9
Control
Perturbation